International Journal of Heat and Mass Transfer 52 (2009) 2749–2758

Contents lists available at ScienceDirect

International Journal of Heat and Mass Transfer

journal homepage: www.elsevier.com/locate/ijhmt

Retrieval of thermal properties in a transient conduction–radiation problem with variable thermal conductivity

Ranjan Das [a], Subhash C. Mishra [b,1,*], R. Uppaluri [c]

[a] Department of Mechanical Engineering, Indian Institute of Technology Guwahati, Guwahati 781039, India
[b] Institute of Fluid Science, Tohoku University, 2-1-1 Katahira, Aoba-ku, Sendai 980-8577, Japan
[c] Department of Chemical Engineering, Indian Institute of Technology Guwahati, Guwahati 781039, India

ARTICLE INFO

Article history:
Received 19 August 2008
Available online 18 February 2009

Keywords:
Parameter retrieval
Conduction–radiation
Participating medium
Lattice Boltzmann method
Finite volume method
Genetic algorithm

ABSTRACT

This article reports an inverse analysis of a transient conduction–radiation problem with variable thermal conductivity. Simultaneous retrieval of parameters is accomplished by minimizing the objective function represented by the square of the difference between the measured and the assumed temperature fields. The measured temperature field is calculated from the direct method involving the lattice Boltzmann method (LBM) and the finite volume method (FVM). In the direct method, the FVM is used to obtain the radiative information and the LBM is used to solve the energy equation. With perturbations imposed on the measured temperature data, minimization of the objective function is achieved with the help of the genetic algorithm (GA). The accuracies of the retrieved parameters have been studied for the effects of the genetic parameters such as the crossover and the mutation rates, the population size, the number of generations and the effect of noise on the measured temperature data. A good estimation of parameters has been obtained.

1. Introduction

Analysis of a heat transfer problem generally involves determination of temperature and/or heat flux distributions from the knowledge of medium properties, and initial and boundary conditions. Such problems are known as direct problems. They are mathematically well-posed, and established methods are available for their solutions. However, in many situations, the knowledge about the temperature and/or heat flux distribution is available, but either the medium properties or the boundary conditions are unknown. Problems of this kind fall under the domain of inverse problems. They are mathematically ill-posed, and their solutions require either some kind of regularization or an efficient optimization method.

Inverse problems find applications in design and analysis of many devices such as furnaces, combustors, turbomachinery, heaters and radiators, etc. The Laplace transform method, the finite element method in conjunction with the least-squares method was employed by Chen and Chang [1] to estimate surface heat flux/temperature from measured temperature inside the solid in an inverse heat conduction problem. Wang et al. [2] have carried out an inverse analysis for turbomachinery blading. Liu and Jiang [3] reconstructed temperature profiles in flames in a combustion study. They used Gauss–Jordan elimination method in the inverse analysis. Erturk et al. [4] have determined the boundary conditions for a radiative enclosure using the conjugate gradient method. Behbahani-nia and Kowsary [5] have estimated heat flux profiles using dual reciprocity boundary element along with sequential function specification scheme. Transient heat source reconstruction from temperature measurements using the Bayesian approach was carried out by Wang and Zabaras [6]. Huang and Wu [7] estimated the temperature at the base of the fin using iterative conjugate gradient method. Woodfield et al. [8] estimated the heat flux using inverse Laplace transformation. Kolehmainen et al. [9] used semi-discrete finite element approximation in conjunction with the Bayesian approach to estimate the heat capacity and the thermal conductivity in a tomographic inverse problem. Lin and Yang [10] determined the strength of the heat source in Fourier and non-Fourier heat conduction problems. They used the finite difference method and the modified Newton–Raphson method. Chiang and Chen [11] applied grey prediction to estimate thermal conductivity in heat conduction problem. Liu [12] estimated the heat source in a conduction problem using genetic algorithm (GA).

In a conduction–radiation problem, the solution of the energy equation can be accomplished by methods such as the finite element method [13], the finite difference method (FDM) [14], the finite volume method (FVM) [15] and the lattice Boltzmann method

* Corresponding author. Tel.: +81 22 217 5270; fax: +81 22 217 5244.
E-mail address: scm_iitg@yahoo.com (S.C. Mishra).
[1] On leave from the Department of Mechanical Engineering, IIT Guwahati, Guwahati 781039, India.

0017-9310/$ - see front matter © 2009 Elsevier Ltd. All rights reserved.
doi:10.1016/j.ijheatmasstransfer.2008.12.009

Nomenclature

a	anisotropy factor
c_p	specific heat at constant pressure
e	propagation speed $(\frac{\Delta x}{\Delta t})$
f_i	particle distribution function in the *i-direction*
f_i^{eq}	equilibrium particle distribution function in the *i-direction*
G	incident radiation
I	intensity
J	objective function
k	thermal conductivity
M	number of rays
n	total number lattices/control volumes
q	heat flux
S	source term
t	dimensional time
T	dimensional temperature
X	length of the geometry
x	space variable

Greek symbols

α	thermal diffusivity
β	extinction coefficient
γ	coefficient for variation in thermal conductivity
γ'	variable thermal conductivity parameter
η	non-dimensional distance
δ	polar angle
ε	emissivity
θ	non-dimensional temperature
κ_a	absorption coefficient
Ω	solid angle
ρ	density
σ	Stefan–Boltzmann constant, 5.67×10^{-8} W/m^2 K^4
σ_s	scattering coefficient
τ	relaxation time in the LBM
ω	scattering albedo
ξ	non-dimensional time

Superscript

$*$	non-dimensional variable
m	index for direction

Subscripts

b	boundary
C	conductive
p	index for lattice node
R	radiative
E, W	east, west

(LBM) [16]. The radiative information required in the problem can be obtained by methods such as the discrete ordinate method (DOM) [17], the discrete transfer method (DTM) [17], the spherical harmonics method [17] and the finite volume method (FVM) [18]. It is observed that most of the available studies involving conduction–radiation heat transfer assume the thermal conductivity to be constant and its variation with the temperature is neglected. However, this assumption fails if there is a large temperature difference in the medium. Chu and Tseng [19] and Talukdar and Mishra [20] have considered the effect of variable thermal conductivity in a conduction–radiation problem. To compute the radiative information, they have used the DOM and the DTM, respectively. The FDM was used for the solution of the energy equation. The consideration of temperature dependent thermal conductivity increases the nonlinearity in the energy equation and the solution of the same becomes more complex [19,20].

In the domain of inverse problems, a transient conduction–radiation problem involving the effect of variable thermal conductivity has not been investigated so far. Therefore, in the present work, we perform an inverse analysis for parameter retrieval in a transient conduction–radiation problem with variable thermal conductivity. For the computation of the radiative information, the FVM [18] is a robust method. In fluid mechanics and heat transfer, the usage of the LBM [21,22] has been found promising. Thus, in the present work, in the direct method, we use the LBM–FVM combination to obtain the temperature field. The divergence of the radiative heat flux is computed using the FVM and the LBM is employed to solve the energy equation. The temperature field obtained in the direct method is taken as the exact (measured) temperature data in the inverse analysis. A set of two parameters such as the extinction coefficient along and the conduction–radiation parameter, the extinction coefficient and the scattering albedo, and the conduction–radiation parameter and the scattering albedo are simultaneously estimated by minimizing the objective function. The GA [6,10–12,23] is an efficient optimization tool, therefore, in the present work, the same is used for the minimization of the objective function.

2. Formulation

Consider an absorbing, emitting and scattering planar medium (Fig. 1). The initial temperature of the system is T_E. For time $t > 0$, the west boundary is maintained at a higher temperature $T_W > T_E$. The thermal conductivity k of the medium is assumed to vary with temperature according to the following expression,

$$k = k_0 + \gamma'(T - T_W) \tag{1}$$

where γ' is the variable thermal conductivity parameter. The energy equation for the problem under consideration is given by,

$$\rho C_p \frac{\partial T}{\partial t} = -\frac{\partial}{\partial x}\left(-k\frac{\partial T}{\partial x}\right) - \frac{\partial q_R}{\partial x} \tag{2}$$

Substituting for k from Eq. (1) into Eq. (2), we get,

$$\rho C_p \frac{\partial T}{\partial t} = [k_0 + \gamma'(T - T_W)]\frac{\partial^2 T}{\partial x^2} + \gamma'\left(\frac{\partial T}{\partial x}\right)^2 - \frac{\partial q_R}{\partial x} \tag{3}$$

If in non-dimensional form, we define, time ξ, distance η, temperature θ, radiative heat flux Ψ_R, coefficient of variation in thermal conductivity γ, conduction–radiation parameter N and incident radiation G^* in the following way,

$$\xi = \alpha\beta^2 t \quad \eta = \beta x \quad \theta = \frac{T}{T_W} \quad \Psi_R = \frac{q_R}{\sigma T_W^4} \quad \gamma = \frac{\gamma' T_W N}{k_0}$$
$$N = \frac{k_0\beta}{4\sigma T_W^3} \quad G^* = \frac{G}{\sigma T_{ref}^4/\pi} \tag{4}$$

Eq. (3) can be written in non-dimensional form as

$$\frac{\partial\theta}{\partial\xi} = \left(1 + \frac{\gamma(\theta - 1)}{N}\right)\frac{\partial^2\theta}{\partial\eta^2} + \frac{\gamma}{N}\left(\frac{\partial\theta}{\partial\eta}\right)^2 - \frac{1}{4N}\frac{\partial\Psi_R}{\partial\eta} \tag{5}$$

In Eq. (5), the divergence of the radiative heat flux is given by,

$$\frac{\partial\Psi_R}{\partial\eta} = 4(1 - \omega)\left(\theta^4 - \frac{G^*}{4\pi}\right) \tag{6}$$

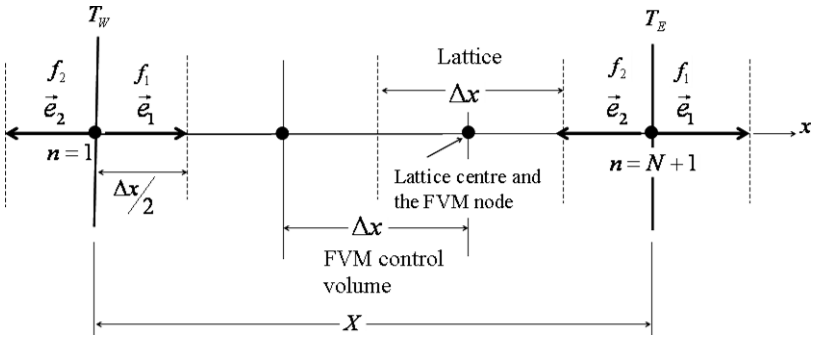

Fig. 1. Schematic of the 1-D planar geometry under consideration along with D1Q2 lattice of the LBM and control volume of the FVM.

In the present work, we compute $\frac{\partial \Psi_R}{\partial \eta}$ using the FVM and the LBM is employed to compute the temperature field in both the direct and the inverse methods. In the inverse method, the optimization is achieved using the GA. Below we provide a brief formulation of the FVM, the LBM and the GA.

2.1. Finite volume method

For a participating medium, the radiative transfer equation in any discrete direction δ^j having direction index j is given by [17,18]

$$\frac{dI^j}{ds^j} = -\beta I^j + S^j \tag{7}$$

where I^j is the intensity in the discrete direction δ^j (where δ is the polar angle). The source term S^j for an absorbing, emitting and anisotropically scattering medium in which anisotropy is approximated by linear anisotropic phase function ($p = 1 + a\cos\delta\cos\delta^{'}$) is given by

$$S^j = \beta(1-\omega)\left(\frac{\sigma T^4}{\pi}\right) + \frac{\beta\omega}{4\pi}(G + a\cos\delta^j q_R) \tag{8}$$

In Eq. (8), the incident radiation G and net heat flux q_R are given by and computed from the following:

$$G = 2\pi\int_{\delta=0}^{\pi} I\sin\delta d\delta \approx 4\pi\sum_{j=1}^{M} I^j \sin\delta^j \sin\left(\frac{\Delta\delta^j}{2}\right) \tag{9}$$

$$q_R = 2\pi\int_{\delta=0}^{\pi} I\cos\delta\sin\delta d\delta \approx 2\pi\sum_{j=1}^{M} I^j \sin\delta^j\cos\delta^j\sin(\Delta\delta^j) \tag{10}$$

where M is the number of discrete points considered over the complete span of the polar angle δ ($0 \leqslant \delta \leqslant \pi$).

In the FVM, for a planar medium, Eq. (7) is resolved along the x-direction and it is integrated over the elemental solid-angle $\Delta\Omega$ to provide

$$\frac{\partial I^j}{\partial x} D_x^j = -\beta I^j \Delta\Omega^j + S^j \Delta\Omega^j \tag{11}$$

In Eq. (11), D_x^j and $\Delta\Omega^j$ are given by

$$D_x^j = 2\pi\sin\delta^j\cos\delta^j\sin(\Delta\delta^j) \tag{12}$$

$$\Delta\Omega^j = 4\pi\sin\delta^j\sin\left(\frac{\Delta\delta^j}{2}\right) \tag{13}$$

Integrating Eq. (11) over a 1-D control volume, we get

$$(I_E^j - I_W^j)D_x^j = -\beta I_P^j dx\Delta\Omega^j + S_P^j dx\Delta\Omega^j \tag{14}$$

where I_E^j and I_W^j are the intensities at the east and the west cell boundaries and I_P^j and S_P^j are the intensity and the source term at the cell centre P in a given direction having index j. If the cell centres intensity $I_P^j = (I_E^j + I_W^j)/2$ then in terms of known intensities, it can be written as

$$I_P^j = \begin{cases} \frac{2D_x^j I_W^j + S_P^j \Delta\Omega^j dx}{2D_x^j + \beta\Delta\Omega^j dx}, D_x^j > 0 \\ \frac{2|D_x^j| I_E^j + S_P^j \Delta\Omega^j dx}{2|D_x^j| + \beta\Delta\Omega^j dx}, D_x^j < 0 \end{cases} \tag{15}$$

While marching from any of the two boundaries, knowledge of the boundary intensity is required, and this for a diffuse-gray boundary having temperature T_b and emissivity ϵ_b, is computed from

Table 1
Effect of number of lattices/control volumes in the direct method (LBM–FVM) and number of directions in the FVM on the variation of steady state (SS) temperature θ; $\varepsilon_E = \varepsilon_W = 1.0$, $\beta = 1.0$, $\omega = 0.5$, $N = 0.01$, $\gamma = 0.50$.

Control volumes/ lattices	Number of directions M_δ	Non-dimensional location		
		$\eta = 0.20$	$\eta = 0.40$	$\eta = 0.80$
Effect of control volumes/lattices				
25	12	0.9019	0.8247	0.6439
50	12	0.8928	0.8401	0.6937
100	12	0.8905	0.8550	0.7392
200	12	0.8900	0.8596	0.7486
Effect of number of directions M_δ				
100	6	0.8377	0.8036	0.7023
100	12	0.8905	0.8550	0.7392
100	24	0.9045	0.8643	0.7429

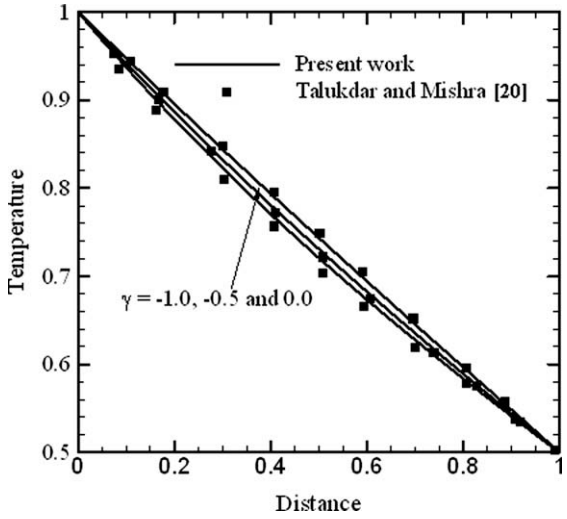

Fig. 2. Validation of the SS temperature θ distribution computed in the present work for the direct problem with that of Talukdar and Mishra [20] for different values of γ; $N = 0.50$, $\beta = 0.1$, $\omega = 0.50$, $\varepsilon_E = 1.0$, $\varepsilon_W = 0.50$.

$$I_b = \frac{\varepsilon_b \sigma T_b^4}{\pi} + \left(\frac{1-\varepsilon_b}{\pi}\right) 2\pi \sum_{j=1}^{M/2} I^j \sin\delta^j \cos\delta^j \sin(\Delta\delta^j) \tag{16}$$

2.2. Lattice Boltzmann method

For a planar medium, with D1Q2 lattice, the discrete Boltzmann equation with the Bhatanagar–Gross–Krook approximation is given by [21,22],

$$\frac{\partial f_i(x,t)}{\partial t} + e_i \nabla f_i(x,t) = -\frac{1}{\tau}\left[f_i(x,t) - f_i^0(x,t)\right] \quad i = 1 \quad \text{and} \quad 2 \tag{17}$$

Table 2
Effect of crossover and mutation rates on the simultaneous retrieval of parameters for a population size of 100; $\varepsilon_E = \varepsilon_W = 1.0$, $\gamma = 0.50$.

Exact values	(P_c, P_m)	$(\pm E)$	Estimated values	% Error
$(N,\beta) = (0.01, 1.0)$ $\omega = 0.50$	(0.3, 0.3)	0.0	(0.0124, 1.1935)	(24.0, 19.35)
		1.0	(0.0067, 0.7938)	(−33.0, 20.62)
		2.0	(0.0157, 1.3259)	(57.0, 32.59)
	(0.8, 0.03)	0.0	(0.0105, 1.0581)	(5.0, 5.81)
		1.0	(0.011, 0.9011)	(10.0, −9.89)
		2.0	(0.0082, 0.8584)	(−18.0, −14.16)
$(N,\omega) = (0.01, 0.5)$ $\beta = 1.0$	(0.8, 0.03)	0.0	(0.0097, 0.5481)	(−3.0, 9.62)
		1.0	(0.0081, 0.6039)	(−19.0, 20.78)
		2.0	(0.0128, 0.3673)	(28.0, −26.54)
$(\beta,\omega) = (1.0, 0.5)$ $N = 0.01$	(0.8, 0.03)	0.0	(0.9673, 0.4705)	(−3.27, −5.90)
		1.0	(0.8903, 0.5806)	(−10.97, 16.12)
		2.0	(1.2932, 0.3890)	(29.32, −22.2)

where f_i is the particle distribution function, f_i^0 is equilibrium particle distribution function, e_i is the velocity and τ is the relaxation time which for the D1Q2 lattice used in a 1-D planar medium (Fig. 1) is given by [21,22],

$$\tau = \frac{\alpha}{|e_i|^2} + \frac{\Delta t}{2} \tag{18}$$

For the D1Q2 lattice, the two velocities and their corresponding weights are given by

$$e_i = \frac{\Delta x}{\Delta t}, \qquad e_2 = -\frac{\Delta x}{\Delta t} \tag{19}$$

$$w_1 = w_2 = \frac{1}{2} \tag{20}$$

After discretization, Eq. (17) can be written as,

$$f(x + e_i\Delta t, t + \Delta t) = f_i(x,t) - \frac{\Delta t}{\tau}\left[f_i(x,t) - f_i^0(x,t)\right] \tag{21}$$

To account for the volumetric radiation, Eq. (21) gets modified to [16],

$$f_i(x + e_i\Delta t, t + \Delta t) = f_i(x,t) - \frac{\Delta t}{\tau}\left[f_i(x,t) - f_i^0(x,t)\right] - \frac{\Delta t w_i}{\rho c_p}\frac{\partial q_R}{\partial x} \tag{22}$$

Once the f_i over all directions are known, temperature is obtained from the following:

$$T(x,t) = \sum_{i=1,2} f_i(x,t) \tag{23}$$

To process Eq. (22), knowledge of equilibrium particle distribution function is required and this is given by,

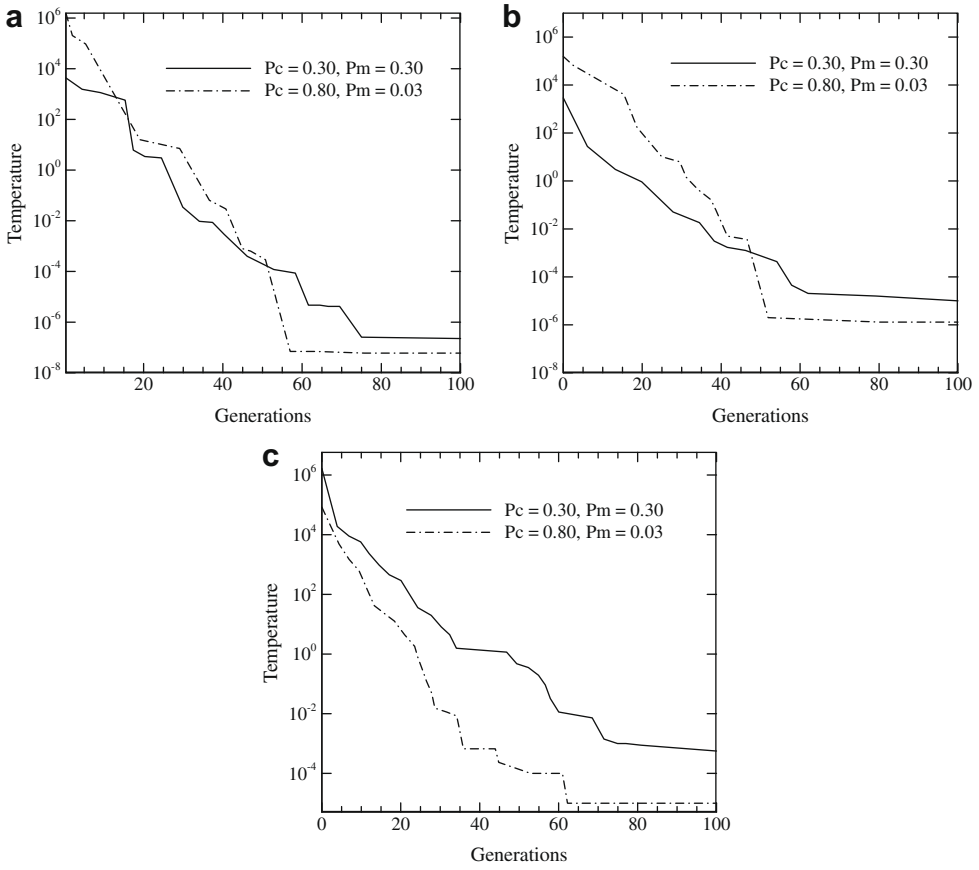

Fig. 3. Comparison of the effect of crossover probability P_c and mutation probability P_m on the variation of the best fitness and number of generations for different measurement errors, (a) $E = 0.0$ (b) $E = 1.0$ and (c) $E = 2.0$; $N = 0.01$, $\beta = 1.0$, $\varepsilon = 1.0$, $\gamma = 0.50$ and $\omega = 0.50$ (estimated values: N and β).

$$f_i^0(x,t) = w_i T(x,t) \tag{24}$$

To account for the temperature dependent thermal conductivity (Eq. (1)), the expression for the relaxation time in Eq. (18) is modified as,

$$\tau = \frac{k/\rho c_p}{|e_i|^2} + \frac{\Delta t}{2} = \frac{k_0 + \gamma'(T - T_W)}{\rho c_p |e_i|^2} + \frac{\Delta t}{2}$$
$$= \frac{k_0}{\rho c_p |e_i|^2} + \frac{\gamma'}{\rho c_p |e_i|^2}(T - T_W) + \frac{\Delta t}{2} \tag{25}$$

Using non-dimensional parameters as defined in Eqs. (4) and (22) can be written as,

$$f_i^*(\eta + e_i^* \Delta\xi, \xi + \Delta\xi) = f_i^*(\eta,\xi) - \frac{\Delta\xi}{\tau^*}\left[f_i^*(\eta,\xi) - f_i^{*0}(\eta,\xi)\right] - \frac{\Delta\xi w_i}{4N}\frac{\partial \Psi_R}{\partial \eta} \tag{26}$$

In Eq. (26), the radiative information $\frac{\partial \Psi_R}{\partial \eta}$ is calculated from Eq. (6). In non-dimensional form the relaxation time τ^* is given by,

$$\tau^* = \frac{1}{(\Delta x^*/\Delta\xi)^2} + \frac{\gamma}{(\Delta x^*/\Delta\xi)^2}(\theta - \theta_W) + \frac{\Delta\xi}{2} \tag{27}$$

The details of the solution procedure and the implementation of boundary conditions in the LBM are given in [16] and the same are not repeated here.

2.3. Genetic algorithm

GA is an iterative optimization tool, which unlike deterministic methods, works with a group of solutions collectively known as the population. Population undergoes gradual refinements in successive generations. The process of the GA is analogous to biological evolutions of any species in which successive generations are conceived, born and raised until they themselves become ready to reproduce. Reproduction, crossover and mutation are the three main steps involved in the GA. After the generation of an initial population and evaluation of its fitness, the process of reproduction starts. The generations having good fitness values are replicated in the next population. Next, the crossover operation starts. In this process, pairs from new strings mate to produce new offspring. The parents are replaced by the newly produced offspring. Finally, through an assigned probability, the mutation operator randomly changes the genes in the string. The process continues until a satisfactory fitness value of the objective function is attained.

In the present work, in the inverse analysis, the objective function is defined as the summation of the squares of the differences between guessed temperature field θ_p and exact temperature field $\tilde{\theta}_p$,

$$J = \sum_{i=1}^{n}\left(\tilde{\theta}_p - \theta_p\right)^2 \tag{28}$$

To account for the effect of measurement errors, random errors to the exact temperature field are added. Thus the temperature θ_{measured} when an error is included is expressed as:

$$\theta_{\text{measured}} = \tilde{\theta} + E \tag{29}$$

where E is a random error between 0 and ±2. When there is no measurement error ($E = 0.0$), $\theta_{\text{measured}} = \tilde{\theta}$ for estimation of unknown

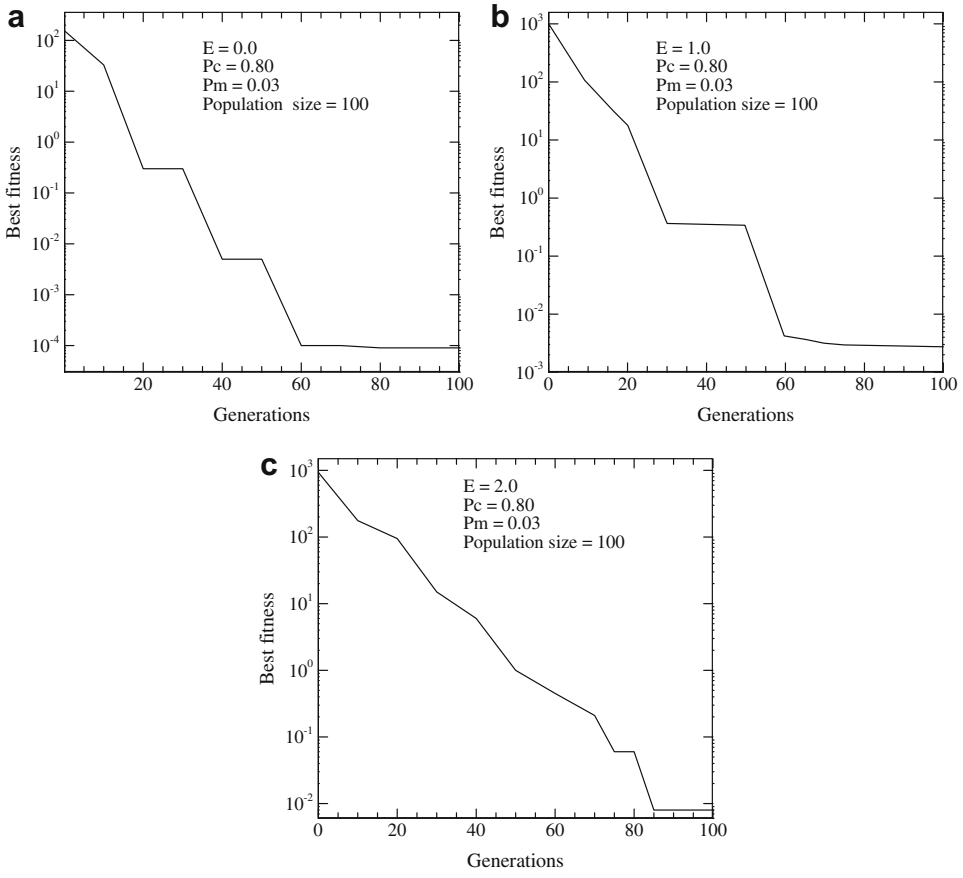

Fig. 4. Comparison of the variation of the best fitness and number of generations for different measurement errors, (a) $E = 0.0$ (b) $E = 1.0$ and (c) $E = 2.0$; $(P_c, P_m) = (0.80, 0.03)$, $N = 0.01$, $\gamma = 0.50$, $\beta = 1.0$, $\varepsilon = 1.0$ and $\omega = 0.50$ (estimated values: N and ω).

parameters, the minimization of the objective function (Eq. (28)) is required.

3. Results and discussion

In the following pages, we provide results of the inverse analysis for the simultaneous retrieval of parameters. Initially the entire system is at a temperature $\theta(\eta,0) = 0.5$. For time $\xi > 0$, the east boundary is kept at the same initial temperature ($\theta_E = 0.5$) and the west boundary is maintained at a higher temperature $\theta_W = 2\theta_E = 1.0$. In the energy equation, the non-dimensional time step $\Delta\xi = 0.0001$ was considered. The steady state (SS) conditions were assumed to have been attained when the temperature difference between two consecutive time levels at each lattice centre did not exceed 1.0×10^{-6}.

In Table 1, we study the effect of lattices/control volumes and number of rays on the SS temperature θ distribution. For this, both the boundaries are assumed to be black. The comparison corresponds to the extinction coefficient $\beta = 1.0$, the scattering albedo $\omega = 0.5$, the conduction–radiation parameter $N = 0.01$ and the coefficient of variation of thermal conductivity $\gamma = 0.5$. It is observed from Table 1 that beyond 100 control volumes and 12 rays, there is no significant change in the temperature θ distributions. Therefore, in the present work, we have provided the results considering 100 control volumes and 12 rays. It is to be noted that in the LBM, the number of lattices remains one more than the number of control volumes in the FVM.

In order to check the accuracy of the direct method (LBM–FVM), in Fig. 2, we compare the SS temperature θ distributions with that given in Ref. [20]. The cold/east boundary is assumed to be black and the emissivity of the hot/west boundary $\varepsilon_W = 0.5$.For extinction coefficient $\beta = 0.1$, the scattering albedo $\omega = 0.5$ and the conduction–radiation parameter $N = 0.5$, this comparison has been shown for three values of thermal conductivity parameter $\gamma = -1.0, -0.50$ and 0.0. It is observed from Fig. 2 that the SS temperature θ distributions obtained from the direct method (LBM–FVM) compare very well with those given in [20] in which the problem was solved using the finite difference method involving implicit scheme and the discrete transfer method.

In the following pages, we present the results for the inverse analysis using the LBM–FVM in conjunction with the GA. For this analysis, at time $\xi > 0.0$, we maintain the non-dimensional temperatures of the west and the east boundaries at $\theta_W = 1.0$ and $\theta_E = 0.5$, respectively. For the set of parameters considered in Table 1, with the SS temperature θ distributions available from the direct method, in the inverse method, we simultaneously estimate two parameters, viz. (β,N), (ω,N) and (β,ω).

To demonstrate the workability of the LBM–FVM–GA in the inverse method, for a population size of 100, in Table 2 we study the effect of the crossover probability P_c and the mutation probability P_m on the accuracy of the simultaneous estimation of the extinction coefficient β and the conduction–radiation parameter N. For measurement errors ($\pm E$) in the range 0–2, the effect has been studied for two cases of P_c and P_m viz. (a) lower value of crossover probability ($P_c = 0.30$) with a higher value of mutation probability ($P_m = 0.30$) and (b) higher value of crossover probability ($P_c = 0.80$) with a much lower value of mutation probability ($P_m = 0.03$). It is observed from Table 2 that for the present study,

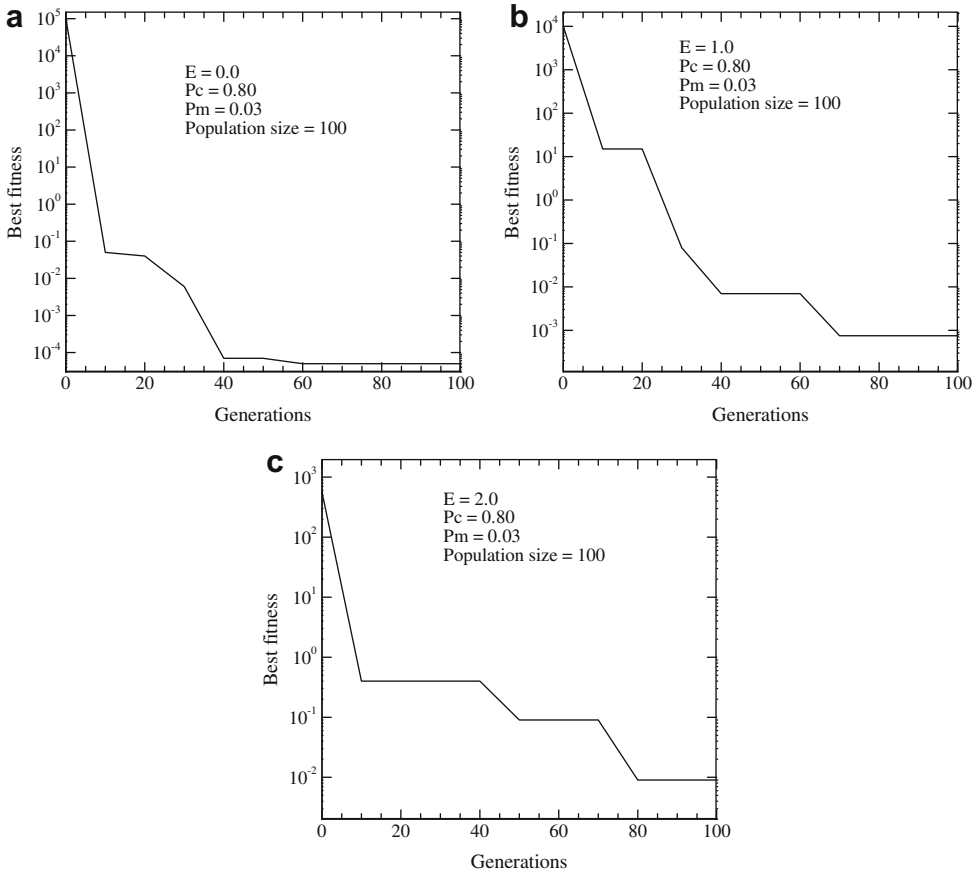

Fig. 5. Comparison of the variation of the best fitness and number of generations for different measurement errors, (a) $E = 0.0$ (b) $E = 1.0$ and (c) $E = 2.0$; $(P_c,P_m) = (0.80,0.03)$, $N = 0.01$, $\beta = 1.0$, $\varepsilon = 1.0$, $\gamma = 0.50$ and $\omega = 0.50$ (estimated values: ω and β).

a higher value of crossover probability (P_c = 0.80) with a much lower value of mutation probability (P_m = 0.03) is desirable. Thus, in the present work, we select the P_c = 0.80 and P_m = 0.03 for simultaneous estimation of other sets of parameters, viz. (β,N), (ω,N) and (β,ω). From Table 2, it is also seen that with P_c = 0.80 and P_m = 0.03, the estimated values of the set of parameters (β,N), (ω,N) and (β,ω) are in good agreement with the exact ones.

For parameters considered in Table 2, in order to study the effects of the crossover probability P_c and the mutation probability P_m on the convergence rate of the best fitness and their effects on the number of generations required for the convergence, we present a comparison in Fig. 3. In the present work, the best fitness is represented by the summation of the errors between the exact temperature field ($\tilde{\theta}$) and the guessed temperature field (θ). Since the present work deals with a transient problem, it is to be noted that the minimization of this objective function need to be carried out at all the time levels including SS. For simultaneous estimation of the extinction coefficient β and the conduction–radiation parameter N, the comparison has been done for three different measurement errors viz. $\pm E$ = 0.0, 1.0 and 2.0. It can be observed that for all the measurement errors ($\pm E$), a crossover probability P_c = 0.8 and a mutation probability P_m = 0.03 provide a minimum value of the best fitness as compared to the other combination of the crossover probability P_c and the mutation probability P_m, i.e., (P_c = 0.30, P_m = 0.30). Further, it can be noticed that in case of (P_c,P_m) = (0.8,0.03), the attainment of the convergence is faster. However, for other combination of P_c and P_m, i.e., (P_c = 0.30, P_m = 0.30), it is also observed that there is no significant change in the variation of the best fitness beyond 100 generations. Thus in the present work, the analysis has been done for a maximum of 100 generations.

In Fig. 4, we present the variation of the best fitness with the number of generations for the simultaneous retrieval of the conduction–radiation parameter N and the scattering albedo ω. The study has been done for three measurement errors ($\pm E$ = 0.0, 1.0 and 2.0). It is observed that the value of the best fitness increases with measurement errors for a fixed number of generations (100 for the present study). It is also noticed that the convergence rate is faster for the case involving least measurement error, i.e., ($\pm E$ = 0.0). This can be explained in the following manner. When the initial population contains large error, the probability that

Table 3
Effect of the population size on the estimation accuracy of simultaneous retrieval of parameters; $\varepsilon_E = \varepsilon_W$ = 1.0, γ = 0.50.

Exact values	Population size	($\pm E$)	Estimated values	% Error
(N,β) = (0.01,1.0)	25	0.0	(0.0161, 1.3617)	(61.0, 36.17)
ω = 0.50		1.0	(0.0022, 1.4321)	(−78.0, 43.21)
		2.0	(0.0014, 0.4803)	(−86.0, −51.97)
	100	0.0	(0.0105, 1.0581)	(5.0, 5.81)
		1.0	(0.011, 0.9011)	(10.0, −9.89)
		2.0	(0.0082, 0.8584)	(−18.0, −14.16)
(N,ω) = (0.01,0.50)	100	0.0	(0.0097, 0.5481)	(−3.0, 9.62)
β = 1.0		1.0	(0.0081, 0.6039)	(−19.0, 20.78)
		2.0	(0.0128, 0.3673)	(28.0, −26.54)
(β,ω) = (1.0,0.50)	100	0.0	(0.9673, 0.4705)	(−3.27, −5.90)
N = 0.01		1.0	(0.8903, 0.5806)	(−10.97, 16.12)
		2.0	(1.2932, 0.3890)	(29.32, −22.2)

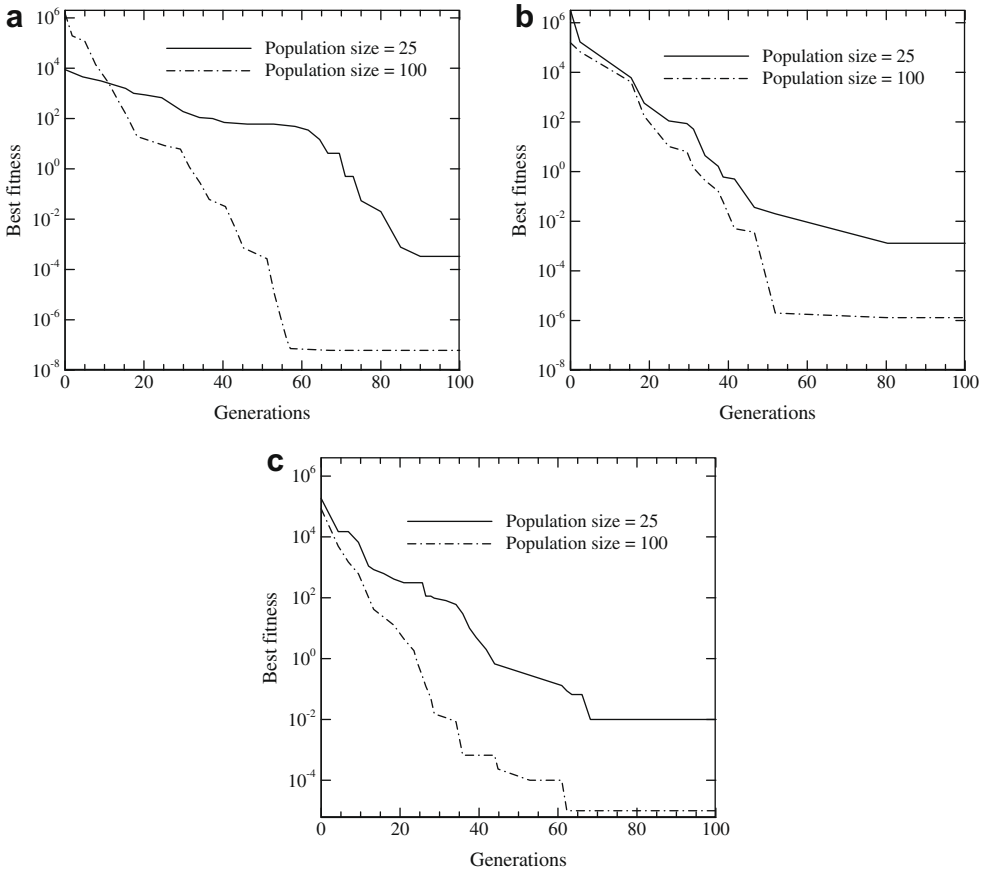

Fig. 6. Comparison of the effect of the population size on the best fitness and number of generations for different measurement errors, (a) E = 0.0 (b) E = 1.0 and (c) E = 2.0; (P_c,P_m) = (0.80,0.03), N = 0.01, β = 1.0, ε = 1.0, γ = 0.50 and ω = 0.50 (estimated values: N and β).

the GA needs large number of generations for tuning the population towards the minimum value becomes more. On the other hand, with the least measurement error, the probability that the population contains more number of fitter individuals is high. Thus, the convergence rate is faster and less number of generations is required.

For the parameters considered in Table 2, we present the variation of the best fitness with number of generations for the simultaneous retrieval of the extinction coefficient β and the scattering albedo ω in Fig. 5. It is observed that for all measurement errors ($\pm E$), the variation is similar to the one observed in Fig. 4. Thus, a similar justification can be provided for the present case also.

In order to study the effect of population size on the accuracy of the estimated parameters in the inverse method, we present a comparison in Table 3. For simultaneous estimation of the extinction coefficient β and the conduction–radiation parameter N, the study has been made for two different population sizes of 25 and 100. For different measurement errors ($\pm E$), the crossover probability P_c and the mutation probability P_m have been taken as 0.80 and 0.03, respectively, because this combination appears to perform better as observed from Table 2 and Figs. 3–5. It is observed from Table 3 that a higher population size gives a more accurate value of the retrieved parameter. This is because, the higher the population size, the more is the probability of getting better individuals in the population. The estimated values of the other set of parameters viz., the scattering albedo ω with the conduction–radiation parameter N, and the extinction coefficient β with the scattering albedo ω agrees well with that of exact ones for a population size of 100 as observed from Table 3.

In order to study the effect of population size on the variation of the best fitness with number of generations, we present a comparison in Fig. 6. For this comparison, the same set of parameters as assumed in Table 3 are taken. It is observed from Fig. 6 that for a higher population size, the attainment of the convergence is faster, i.e., it requires less number of generations for the convergence. However, it is also noticed that the value of the best fitness is considerably less for a greater population size. This establishes the fact that, if more number of good individuals are present in the population then the estimation accuracy also improves. It is also noticed from Fig. 6 that for all measurement errors, there is no change in the value of the best fitness beyond 100 generations.

For different measurement errors ($\pm E$ = 0.0, 1.0 and 2.0), the variation of the best fitness with the number of generations for a population size of 100 and $(P_c, P_m) = (0.80, 0.03)$ in case of the simultaneous estimation of the scattering albedo ω along with the conduction–radiation parameter N and for the simultaneous estimation of the extinction coefficient β and the scattering albedo ω has already been shown in Figs. 4 and 5, respectively. Thus, the details of the same are not repeated here.

In order to demonstrate the accuracy of the estimated parameters obtained in the inverse method, in Fig. 7, we compare temperature θ distributions computed using the direct method and the inverse method. This comparison corresponds to a measurement error $\pm E$ = 2.0. For the selected values of the crossover probability P_c and the mutation probability P_m which in the present study is 0.80 and 0.03, respectively, it is sufficient to compare temperature θ distribution corresponding to $\pm E$ = 2.0. This is because the case $\pm E$ = 2.0 contains a maximum error in the estimated values as com-

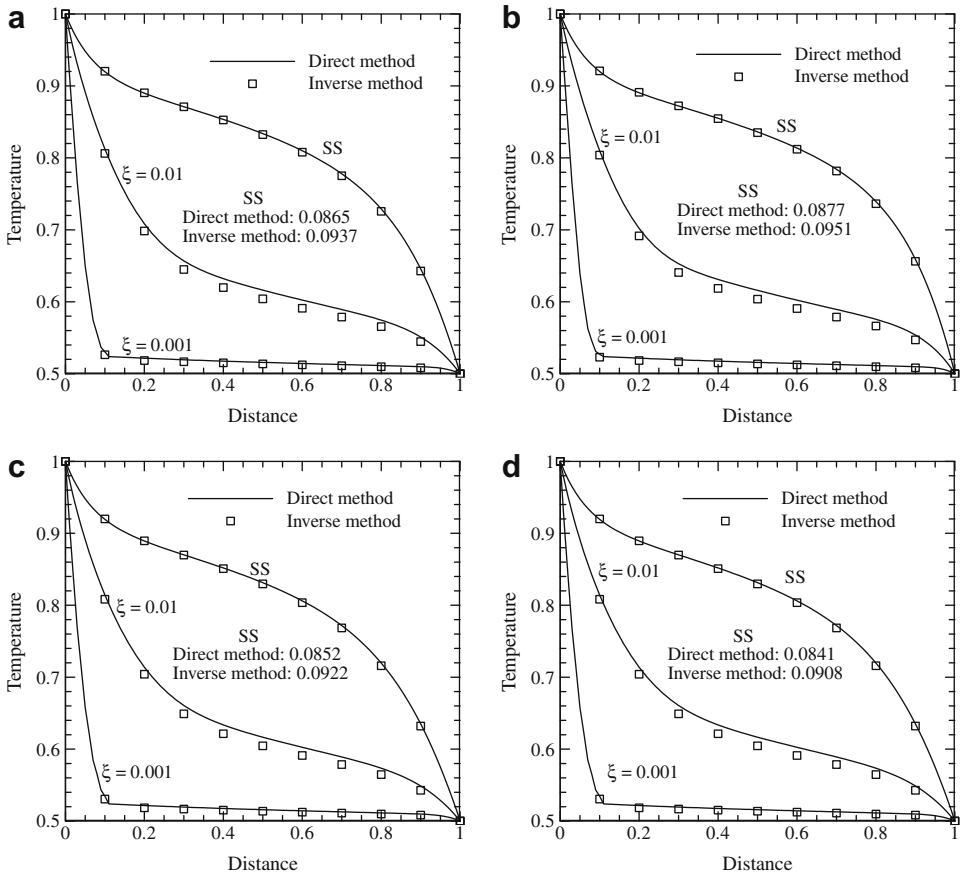

Fig. 7. Comparison of the temperature θ distributions obtained from the direct method and the inverse method with a measurement error, E = 2.0 for (a) γ = 0.0 (b) γ = 0.5 (c) γ = −0.5 and (d) γ = −1.0; ε = 1.0, β = 1.0, ω = 0.5, γ = 0.50 and N = 0.01 (estimated values are N and ω).

pared to other sets of ±E. It is observed from Fig. 7 that temperature θ distributions computed using the direct method and the inverse method are in excellent agreement with each other.

In Fig. 8, we present the variation of the estimated parameters with the number of generations. For all three sets of estimated parameters viz. $(N,\beta) = (0.01, 1.0)$, $(N,\omega) = (0.01, 0.5)$ and $(\beta,\omega) = (1.0, 0.5)$, the results are presented for the case corresponding to a population size of 100, $\varepsilon_E = \varepsilon_W = 1.0$, $\gamma = 0.50$ and $(\pm E) = 0.0$. In each case, it is noticed that the estimated parameter undergo gradual refinement in successive generations. At the end of 100 generations, it is also noticed from Fig. 8 that the exact and the estimated values are in excellent agreement with each other.

In order to study the effect of the CPU time involved in the direct method and the inverse method, we present a comparison in Table 4. The comparison has been done for three different measurement errors viz., ±E = 0.0, 1.0 and 2.0. All runs were carried out on 2.8 GHz CPU (Pentium© 4 with 248 MB RAM). It is evident from Table 4 that in the inverse method the CPU time is approximately 1500 times more than that required in the direct method. This is due to the reason that in the inverse method, the GA starts with a random generation of the initial population. The values of the estimated parameters corresponding to this initial population deviates greatly with respect to the actual ones. Thus, to attain the converged solution, the algorithm has to undergo a series of generations and for a particular generation, in the GA loop, there are a number of processes involved. Therefore, in the inverse method, the CPU time is considerably larger than the direct method.

4. Conclusions

An inverse method was used for simultaneous retrieval of parameters in a transient conduction–radiation problem with variable thermal conductivity. Two of the parameters such as the extinction coefficient, the scattering albedo and the conduction–radiation parameter were simultaneously estimated and they were compared with their exact values. Effects of different genetic parameters such as the crossover and the mutation probabilities, the population size and the number of generations were studied. Effect of measurement errors on the accuracy of the retrieved parameters was also investigated. A comparison of CPU times in-

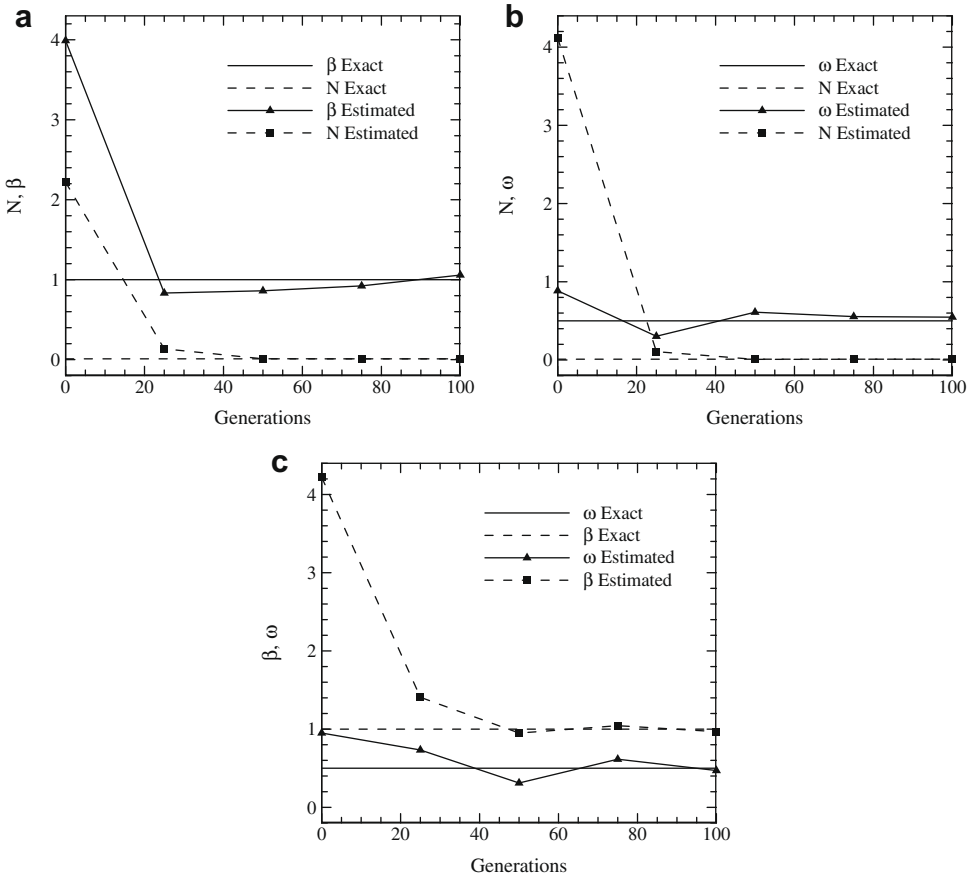

Fig. 8. Variation of estimated values of the retrieved parameters with number of generations (a) $(N,\beta) = (0.01, 1.0)$, (b) $(N,\omega) = (0.01, 0.5)$ and (c) $(\beta,\omega) = (1.0, 0.5)$; $\varepsilon_E = \varepsilon_W = 1.0$, $\gamma = 0.50$, population size = 100, $(P_c, P_m) = (0.8, 0.03)$.

Table 4
Comparison of CPU times required in the direct and the inverse method for population size of 100 and $(P_c, P_m) = (0.80, 0.03)$ for SS temperature θ; $\omega = 0.50$, $\varepsilon_E = \varepsilon_W = 1.0$, $\gamma = 0.50$.

Exact values	Estimated values	(±E)	CPU time (s)		Ratio of CPU times
			Direct method	Inverse method	
$(N,\beta) = (0.01, 1.0)$	(0.0105, 1.0581)	0.0	9.781	14799	1513.03
	(0.011, 0.9011)	1.0		15012	1534.81
	(0.0082, 0.8584)	2.0		15758	1611.08

volved in the direct and the inverse method was also done. The accuracy of the estimated parameters was checked by comparing the temperature distributions obtained using the direct and the inverse method. The LBM–FVM in conjunction with the GA has been found to provide reasonably good estimates for the unknown parameters in a transient conduction–radiation problem with temperature dependent thermal conductivity.

Acknowledgement

Research grant for the work received from the Defense Research and Development Laboratory, Hyderabad is duly acknowledged.

References

[1] H.T. Chen, S.M. Chang, Application of the hybrid method to inverse heat conduction problems, Int. J. Heat Mass Transfer 33 (1990) 621–628.
[2] Z. Wang, R. Cai, H. Chen, X. Jia, A three-dimensional inverse method using Navier–Stokes equations for turbomachinery blading, Inv. Prob. Sci. Eng. 8 (2000) 529–551.
[3] L.H. Liu, J. Jiang, Inverse radiation problem for reconstruction of temperature profile in axisymmetric free flames, J. Quant. Spectrosc. Radiat. Transfer 70 (2001) 207–215.
[4] H. Erturk, O.A. Ezekoye, J.R. Howell, The application of an inverse formulation in the design of boundary conditions for transient radiative enclosure, J. Heat Transfer 124 (2002) 1095–1102.
[5] A. Behbahani-nia, F. Kowsary, A dual reciprocity BE-based sequential function specification solution method for inverse heat conduction problems, Int. J. Heat Mass Transfer 47 (2004) 1247–1255.
[6] J. Wang, N. Zabaras, Using Bayesian statistics in the estimation of heat source in radiation, Int. J. Heat Mass Transfer 48 (2005) 15–29.
[7] C.H. Huang, H.H. Wu, An iterative regularization method in estimating the base temperature for non-Fourier fins, Int. J. Heat Mass Transfer 49 (2006) 4893–4902.
[8] P.L. Woodfield, M. Monde, Y. Mitsutake, On estimating thermal diffusivity using analytical inverse solution for unsteady one-dimensional heat conduction, Int. J. Heat Mass Transfer 50 (2007) 1202–1205.
[9] V. Kolehmainen, J.P. Kaipio, H.R.B. Orlande, Reconstruction of thermal conductivity and heat capacity using a tomographic approach, Int. J. Heat Mass Transfer 50 (2007) 5150–5160.
[10] D.T.W. Lin, C. Yang, The estimation of the strength of the heat source in the heat conduction problems, Appl. Math. Model. 31 (2007) 2696–2710.
[11] J.Y. Chiang, C.K. Chen, Application of grey prediction to inverse nonlinear heat conduction problem, Int. J. Heat Mass Transfer 51 (2008) 576–585.
[12] F.B. Liu, A modified genetic algorithm for solving the inverse heat transfer problem of estimating plan heat source, Int. J. Heat Mass Transfer 51 (2008) 3745–3752.
[13] S.M.H. Sarvari, J.R. Howell, S.H. Mansouri, Inverse boundary design conduction–radiation problem in irregular two-dimensional domains, Numer. Heat Transfer B 44 (2003) 209–224.
[14] F. Asllanaj, A. Milandri, G. Jeandel, J.R. Roche, A finite difference solution of non-linear systems of radiative–conductive heat transfer equations, Int. J. Numer. Methods Eng. 54 (2002) 1649–1668.
[15] S.V. Patankar, Numerical Heat Transfer and Fluid Flow, first ed., Hemisphere Publishing Corp., Washington, DC, 1980.
[16] S.C. Mishra, H.K. Roy, Solving transient conduction–radiation problems using the lattice Boltzmann method and the finite volume method, J. Comput. Phys. 223 (2007) 89–107.
[17] M.F. Modest, Radiative Heat Transfer, second ed., Academic Press, New York, 2003.
[18] J.C. Chai, H.S. Lee, S.V. Patankar, Finite volume method for radiation heat transfer, J. Thermophys. Heat Transfer 8 (1994) 419–425.
[19] H.S. Chu, C.J. Tseng, Conduction–radiation interaction in absorbing, emitting and scattering media with variable thermal conductivity, J. Thermophys. Heat Transfer 6 (1992) 537–540.
[20] P. Talukdar, S.C. Mishra, Transient conduction and radiation heat transfer with variable thermal conductivity, Numer. Heat Transfer A 41 (2002) 851–867.
[21] D.A. Wolf-Gladrow, Lattice-Gas Cellular Automata and Lattice Boltzmann Models: An Introduction, Springer-Verlag, Berlin–Heidelberg, 2000.
[22] S. Succi, The Lattice Boltzmann Method for Fluid Dynamics and Beyond, Oxford University Press, New York, 2001.
[23] J.H. Holland, Adaptation in Natural and Artificial Systems, University of Michigan, Ann Arbor, MI, 1975.